Effects of particle morphology and surface hydrogenation on the phase stability of TiO_2

A. S. Barnard[1,*] and P. Zapol[1,2,†]
[1]*Center for Nanoscale Materials, Argonne National Laboratory, Argonne, Illinois 60439, USA*
[2]*Materials Science and Chemistry Divisions, Argonne National Laboratory, Argonne, Illinois 60439, USA*
(Received 17 February 2004; revised manuscript received 27 July 2004; published 3 December 2004)

Titanium dioxide nanoparticles are currently receiving a lot of attention due to their inherent suitability for advanced photochemical applications. Size, phase, and morphology of the nanoparticles are the critical parameters determining their performance in particular applications. A thermodynamic model devised to describe the shape of nanoparticles as a function of size has been used to predict the phase stability of titanium dioxide nanoparticles, with particular attention given to the crossover of stability between the anatase and rutile phases. Density functional calculations were used to accurately determine surface energies and surface tensions. The effects of nanocrystal morphology on the phase transition are addressed and comparisons drawn with previously reported studies. Further, the model has been applied to titanium dioxide nanoparticles with hydrogenated surfaces, to investigate the effects of surface passivation on the equilibrium shape and the phase transition, and show that surface passivation has an important impact on nanocrystal morphology and phase stability. The results show that surface hydrogenation induces significant changes in the shape of rutile nanocrystals, but not in anatase, and that the size at which the phase transition may be expected increases dramatically when the under-coordinated surface titanium atoms are H-terminated.

DOI: 10.1103/PhysRevB.70.235403 PACS number(s): 61.46.+w, 64.70.Nd, 68.35.−p, 78.67.Bf

I. INTRODUCTION

Titanium dioxide (TiO_2), although widely used as an advanced semiconductor for many years, is now receiving additional attention as TiO_2 nanoparticles are proving to be highly applicable in advanced photochemical applications;[1] especially interfacing with organic molecules[2] and DNA.[3] Recently, the size, phase and morphology of the TiO_2 nanoparticles have been found to be critical parameters determining their suitability for particular applications.[4–6] For example, x-ray analysis has shown that distortions in the surface structure of anatase nanocrystals are responsible for the binding of small molecules,[4,7] and quantitative measurements of adsorption from solution exhibit a 70-fold increase in the adsorption coefficient when a variety of organic acids are adsorbed onto 6 nm as compared to 16 nm TiO_2 nanoparticles.[8]

Although at ambient pressures and temperatures, the rutile phase is more thermodynamically stable than the anatase phase,[9] anatase has been found to be a majority product of industrial sol-gel, and aerosol syntheses of nanocrystalline TiO_2.[10] It is believed that during coarsening of the nanocrystalline anatase, anatase transforms to rutile at a critical size, above which the rutile particles coarsen more quickly than any remaining anatase.[10] These experimental findings indicate that anatase nanocrystals of only a few nanometers in diameter may be more stable than rutile. Therefore, a detailed understanding of the thermodynamic phase stability of nanocrystalline TiO_2 nanocrystals is not only useful in the control of processes such as nucleation and grain growth, but is also essential in facilitating new applications and technologies.

A number of studies have examined the size dependence of the anatase to rutile phase transition. Zhang and Banfield (and colleagues) have been very active in this area, deriving both thermodynamic[11–13] and kinetic[13–15] approaches. Their thermodynamic analysis was based on a (temperature dependent) free energy model for the stability of spherical anatase and rutile nanoparticles as a function of the particle radius.[11] This study predicted that anatase will be thermodynamically preferred below approximately 14 nm in diameter, but unfortunately the model failed to account for the different number of TiO_2 units in anatase and rutile nanocrystals of the same diameter. Their kinetic analysis was based on an interface nucleation and constant growth model and examined the size dependence of phase transition rates,[14] interface and surface nucleation,[15] and the size dependent phase stability of anatase, brookite and rutile nanocrystals.[13,16]

It has also been shown that nanocrystalline TiO_2 may be phase selected by careful control of the particle size, as well as other experimental conditions,[17–20] such as temperature.[21,22] The anatase-to-rutile phase transition was also found to be affected by doping TiO_2 with manganese ions,[23] niobium,[24] and cesium dioxide.[25]

In addition to the control of the size of anatase nanocrystals, the shape may also be manipulated,[19,26,27] which may in turn enhance the adsorption properties of the nanocrystals by exposing and increasing the effective area of preferred surface facets. It is important to note that nanoparticles of TiO_2 are not necessarily spherical.[28] High resolution transmission electron microscopy (HRTEM) evidence has clearly shown that the tetragonal bipyramidal morphology of anatase nanocrystals persists down to 3–5 nm in diameter,[29] i.e., in the size regime at which anatase has been identified as being thermodynamically preferred (over rutile). Similarly, the morphology of larger (~20 nm) rutile nanocrystals can be discerned from the TEM images of Aruna *et al.*[30] Therefore, a general description of the phase stability of these nanomaterials requires the inclusion of nanocrystal shape, as well as size, if tailoring of nanoparticles is to be a viable exercise.

Recently we have derived a thermodynamic model[31] based on the free energy of (arbitrary) nanocrystals as a function of size and shape. In principle, this free energy model may be applied to any material, and may be used to predict phase transitions by comparing results for respective polymorphs. In the present study, this model has been used to examine the relative phase stability of clean nanoscale anatase and rutile, and consider the effects of nanocrystal morphology on the phase transition.

The role of hydrogen on anatase and rutile surfaces is still somewhat unclear, although it is possible that so-called experimental clean surfaces may to some extent be covered with hydrogen.[32] Although it has been found that rutile surfaces do not interact strongly with hydrogen,[33] and that molecular hydrogen does not absorb at ambient temperatures,[34] low energy ion scattering experiments indicate that atomic hydrogen does bind to the rutile (110) surface at room temperature.[34] However, TiO_2 nanoparticles in highly acidic solutions have H-terminated surfaces.

Therefore, as the model takes as input the possible geometries of the nanocrystal morphology, the surface free energy (γ) and the surface tension (σ, which has a small but important effect on the calculation of the anatase to rutile phase transition[35]) for each of the facets present on the crystal, we have generated a consistent set of surface energy and surface tension values for clean, partially and fully hydrogenated stoichiometric low index (1×1) surfaces of both anatase and rutile, using *ab initio* methods.

II. METHODOLOGY

The surface structure and energetics of the low index (100), (110), (101), and (001) surface of anatase and rutile were considered by comparing highly accurate first principles calculations of the total energy of two dimensional slabs with the energy of a bulk TiO_2 lattice as outlined in Sec. IV. The slabs, comprising three trilayers, were generated by the addition of a 15 Å vacuum layer in the crystallographic plane of interest.

The surface slabs were then passivated by either fully ($\theta=1$) or partially ($\theta=0.5$) hydrogenating the cleaved surfaces. The fully hydrogenated surfaces were obtained by terminating all under-coordinated sites, replacing the missing neighbors of both the Ti and O atoms on the surface with hydrogen atoms, whereas the partially hydrogenated surfaces were obtained by terminating only the surface twofold coordinated bridging O atoms with hydrogen. All bulk and surface structures were relaxed prior to calculation of the total energies.

The first principles calculations have been carried out using density functional theory (DFT) within the generalized-gradient approximation (GGA), with the exchange-correlation functional of Perdew and Wang (PW91).[36] This has been implemented via the Vienna *Ab initio* Simulation Package (VASP),[37,38] which spans reciprocal space with a plane-wave basis up to a kinetic energy cutoff of 270 eV. We have used the linear tetrahedron method (LTM) with a $4\times4\times4$ Monkhorst-Pack *k*-point mesh, for both the initial relaxations of the TiO_2 slabs, and the final calculation of surface energies and surface tensions. Although this choice of *k*-mesh results in some superfluous *k* points in the nonperiodic direction of the surface slabs, it was found that the inclusion of these *k* points is more consistent with the LTM.

The electronic relaxation technique used here is an efficient matrix-diagonalization routine based on a sequential band-by-band residual minimization method of single-electron energies,[39,40] with direct inversion in the iterative subspace, whereas the ionic relaxation involves minimization of the Hellmann-Feynman forces. During the relaxations we have used ultrasoft, gradient-corrected Vanderbilt-type pseudopotentials (US-PP)[41,42] and real-space projected wave function (to decrease the computational cost), and have relaxed the total energy to a convergence of 10^{-4} eV. The following (final) energy calculations were then performed using the projected augmented wave (PAW) potentials,[43] with a basis set increased to a cutoff of 350 eV and reciprocal-space projected wave function (to improve accuracy), also to an energy convergence of 10^{-4} eV. PAW potentials are generally considered to be more accurate than the ultrasoft pseudopotentials,[44] since the radial cutoffs (core radii) are smaller than the radii used for the US pseudopotentials, and the fact that the PAW potentials reconstruct the exact valence wave function with all nodes in the core region.

III. SURFACE STRUCTURE

The surface science of titanium dioxide, both anatase and rutile TiO_2, has been extensively investigated (both experimentally and theoretically) and is reasonably well understood.[32] Although numerous studies have already been undertaken by other authors on the (1×1) surface structure and surface energy of stoichiometric anatase[45–47] and rutile,[47–49] a consistent set of surface energies and tensions for both phases (calculated using the same theoretical technique and convergence criteria) is required to provide a suitable input for the phase stability model. To this end, the surface free energy and surface tension has been recalculated for the relaxed low index surfaces to create a complete, uniform set. The structure of the relaxed surfaces is also presented, for the purposes of comparison with other studies. The (100), (110), (101), and (001) surfaces have been selected for inclusion since they may be examined in a straight-forward manner, the results may be verified via comparison with other studies,[32] and these surfaces are known to dominate the Wulff construction[47] and the shape of anatase and rutile crystals both nanoscopically[29,30] and macroscopically. The studies selected for explicit comparison[46,48] herein have been chosen as the authors of these papers also undertook complete studies of the structure and energetics of all low index surfaces of anatase[46] and rutile,[48] respectively.

As mentioned above, the role of hydrogen in structure and stability of these surfaces is still uncertain, although nanoparticles in strong acidic solutions may be H-terminated. Leconte *et al.*[50] examined the structure and energetics of hydrogen on the rutile (110) surface using *ab initio* methods. Their study concluded that H_2 would undergo a heterolytic cleavage and the resulting fragments would adsorb differently. They showed that the proton would adsorb to the oxygen of the uppermost atomic layer, and the hydride-type ion onto

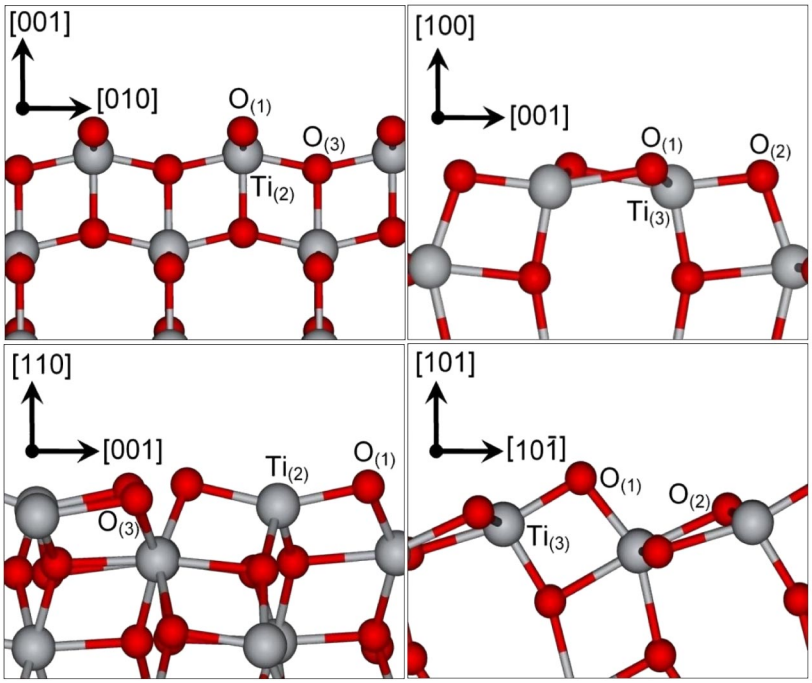

FIG. 1. (Color online) The relaxed anatase (001) surface (top left), (100) surface (top right), (110) surface (lower left), and (101) surface (lower right), with the atoms occupying the atomic layers (denoted by the subscript) of the uppermost trilayer labelled according to Table I.

the Ti atoms of the surface trilayer. Their study indicated that the most favorable surface structure involved all the hydrogen atoms being adsorbed as protons onto outer oxygen atoms,[50] akin to atomic hydrogen adsorption. This configuration corresponds to the partially hydrogenated (110) rutile surface discussed in Sec. III D.

A. Clean anatase surfaces

The surface trilayer of the (001) and (100) surfaces of anatase (see Fig. 1, upper left and upper right images, respectively), contains fivefold coordinated Ti atoms and twofold and threefold coordinated oxygen atoms. Each of these atoms has been labelled in Fig. 1, according to species, with the subscript denoting the atomic layer with respect to the vacuum so that layer (1) is the outermost layer of the surface TiO_2 trilayer. In the case of the (001) surface, the oxygen occupying the third atomic layer ($O_{(3)}$) is threefold coordinated, whereas the outermost oxygen atom ($O_{(1)}$) is twofold coordinated. In each case the labelled $Ti_{(2)}$ atoms are fivefold coordinated. Calculated displacements of these atoms in the uppermost trilayer of the anatase (001) and (100) surfaces are given in Table I, and are compared with the DFT PBE results of Lazzeri *et al.*[46]

The (110) surface shown at the lower left corner of Fig. 1, contains fourfold coordinated Ti atoms ($Ti_{(2)}$) and twofold coordinated oxygen atoms ($O_{(1)}$ and $O_{(3)}$) within the first trilayer. It is important to note that the atoms of the first trilayer are grouped in linear O-Ti-O units [parallel to the (001) direction] in the ideal bulk truncated surface, however the oxygen atoms display different displacements upon relaxation, and are no longer equivalent (normal to the surface) in the final structure.

Finally, the (101) surface containing fivefold Ti atoms ($Ti_{(3)}$) and twofold ($O_{(1)}$) and threefold ($O_{(2)}$) coordinated oxygen atoms (shown at the lower right corner of Fig. 1), displays the characteristic sawtooth profile perpendicular to the (010) direction. These surfaces are also characterized in Table I.

In agreement with the results of Lazzeri *et al.*,[46] trends in the relaxation of the various anatase surfaces involve the outward displacement of the fully coordinated oxygen atoms and bridging under-coordinated oxygen atoms.

TABLE I. Displacements (in Å), normal to the surface, of atoms in the uppermost trilayer of the low index surface of anatase. Comparisons have been drawn with the DFT PBE results of Lazzeri *et al.* (Ref. 46).

Surface	Label	Coordination	This study	Ref. 46
(001)	$O_{(1)}$	2	0.20	0.08
	$Ti_{(2)}$	5	0.04	−0.06
	$O_{(3)}$	3	0.05	−0.02
(100)	$O_{(1)}$	3	0.18	0.18
	$O_{(2)}$	2	0.04	0.02
	$Ti_{(3)}$	5	−0.16	−0.16
(110)	$O_{(1)}$	2	0.28	0.23
	$Ti_{(2)}$	4	−0.29	−0.37
	$O_{(3)}$	2	−0.08	−0.08
(101)	$O_{(1)}$	2	0.06	−0.02
	$O_{(2)}$	3	0.28	0.19
	$Ti_{(3)}$	5	−0.12	−0.18

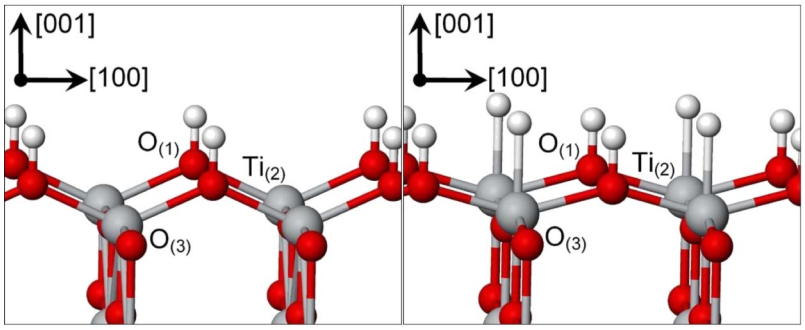

FIG. 2. (Color online) The relaxed, partially hydrogenated anatase (001) surface (left) and fully hydrogenated (001) surface (right). The atoms of the uppermost trilayer labelled according to Table II (atomic layers are denoted by the subscript).

B. H-terminated anatase surfaces

An extensive literature search failed to find any previous work characterizing the structure of the hydrogen terminated surface of anatase; therefore the analysis of relaxed low index anatase surfaces is presented without comparison. In the following description of the remaining anatase surfaces each atom has been labelled in Figs. 2–4, according to species, with the subscript once again denoting the atomic layer with respect to the vacuum.

The partially hydrogenated and fully hydrogenated surface trilayers of the anatase (001) surfaces are shown in Fig. 2 (left and right images, respectively). In the case of the partially hydrogenated surface, only the under-coordinated bridging oxygens of the uppermost atomic layer were terminated with hydrogen, and the surface relaxed. This resulted in a significant outward displacement of both the $O_{(1)}$ and $O_{(3)}$ atoms. The displacement of the $O_{(3)}$ atoms with respect to the bulk indicates that the entire surface trilayer underwent an outward relaxation, which was somewhat compensated by an inward relaxation (toward the bulk) of the titanium atoms, resulting in a minor net outward relaxation of the $Ti_{(2)}$ atoms. For the fully hydrogenated surface (where the under-coordinated $Ti_{(2)}$ atoms were also terminated with hydrogen), the magnitudes of the outward displacement of these atoms are given in Table II along with the O-H and Ti-H bond lengths, and a comparison with previously reported results for the clean anatase (001) surface.

In the case of the (100) surface, the partially hydrogenated and fully hydrogenated surfaces (shown in the left and right images of Fig. 3, respectively) also exhibited an increased outward relaxation compared with the clean surface. The H-terminated $O_{(1)}$ bridging oxygens of the partially hydrogenated surface exhibited a considerable outward relaxation of 0.39 Å (double that of the clean surface), but $Ti_{(3)}$ atoms exhibited an inward relaxation of −0.10 Å. This separation between the atoms of the surface trilayer is reduced when the under-coordinated $Ti_{(3)}$ atoms were also capped with hydrogen (in the fully hydrogenated surface), as the titanium atoms are drawn outward by the terminating hydrogens (see Table II).

When the (101) surface is partially hydrogenated (the left image in Fig. 4) the displacement of the bridging $O_{(1)}$ oxygen atoms changed little, however the outward relaxation of the $O_{(2)}$ atoms was found to increase by 0.15 Å, compared to the clean surface. The results for the fully hydrogenated (101) surface (the right image in Fig. 4) were found to be more similar to the clean surface than the partially hydrogenated surface, with the exception of the $Ti_{(3)}$ atom which (like the other anatase surfaces) was drawn outward by the hydrogen termination. This surface is also characterized in Table II.

In both the partially and fully hydrogenated cases, the (110) surface of anatase was found to deteriorate upon relaxation (becoming a disordered structure), involving the breaking of surface bonds and symmetry and resulting in the desorption of OH molecules. Hence, the resulting surface could no longer be characterized as anatase, rendering it unsuitable for use in the phase stability model presented in the next section.

C. Clean rutile surfaces

In this section, the atom labelling convention used in the previous section for the anatase surfaces has been reapplied to rutile. The results of all low index rutile surface relaxations are listed in Table III, and compared with the DFT LDA results of Ramamoorthy *et al.*[48]

In contrast to anatase, the outermost trilayer of the rutile (001) surface contains exclusively fourfold coordinated Ti

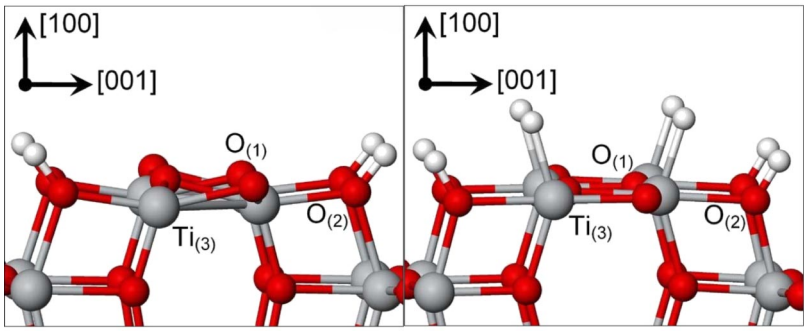

FIG. 3. (Color online) The relaxed, partially hydrogenated anatase (100) surface (left) and fully hydrogenated (100) surface (right). The atoms of the uppermost trilayer labelled according to Table II (atomic layers are denoted by the subscript).

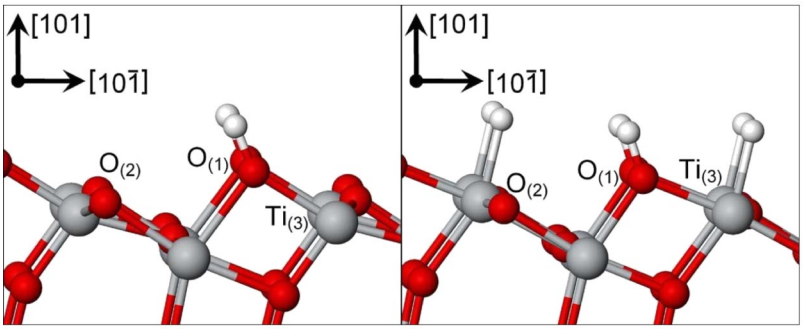

FIG. 4. (Color online) The relaxed, partially hydrogenated anatase (101) surface (left) and fully hydrogenated (101) surface (right). The atoms of the uppermost trilayer labelled according to Table II (atomic layers are denoted by the subscript).

atoms with twofold and threefold coordinated O atoms (see upper left image of Fig. 5). The ideal bulk terminated surface is flat, with O atoms aligned with the equatorial planes perpendicular to the surface. Upon relaxation, the surface Ti atoms contract inward significantly, whereas the outward (inward) relaxations of the $O_{(1)}$ ($O_{(3)}$) atoms are relatively minor in comparison.

The corrugated (100) surface (upper right corner of Fig. 5) contains fivefold coordinated Ti atoms, with chains of twofold coordinated O atoms (bridging O atoms) in the uppermost atomic layer ($O_{(1)}$). A small outward relaxation for the $Ti_{(2)}$, perpendicular to the surface was observed, although it was less than for the O atoms.

The (110) surface (lower left of Fig. 5) contains inequivalent Ti atoms lying in a centered rectangular arrangement. The atoms denoted as $Ti_{(2a)}$ are sixfold coordinated, while the atoms denoted as $Ti_{(2b)}$ are fivefold coordinated. Around the $Ti_{(2a)}$ atoms chains of twofold coordinated bridging $O_{(1)}$ atoms are aligned along the [001] direction, while rows of threefold coordinated $O_{(3)}$ atoms connect the $Ti_{(2a)}$ and $Ti_{(2b)}$ atoms. The dominant relaxations in this case are those perpendicular to the surface, characterized by inward relaxations of the under-coordinated atoms are drawn and outward relaxations of the fully coordinated atoms. The results of the current study (see Table III) are in good agreement with the surface x-ray diffraction results of Charlton *et al.*,[51] where displacements of -0.27 ± 0.08, 0.12 ± 0.05, -0.16 ± 0.05, and 0.05 ± 0.05 Å were reported for the $O_{(1)}$, $Ti_{(2a)}$, $Ti_{(2b)}$, and $O_{(3)}$ atoms, respectively.

Finally, the (011) surface (lower right of Fig. 5), has a ridgelike structure, with fivefold coordinated Ti atoms with in the uppermost trilayer ($Ti_{(2)}$). The bonds between the uppermost O atoms and these Ti atoms form two symmetrical pairs, creating zig-zag chains of twofold coordinated O atoms (labelled $O_{(1a)}$ and $O_{(1b)}$), and threefold coordinated surface O atoms (labelled $O_{(3a)}$ and $O_{(3b)}$) in the first and third atomic layers, respectively. The relaxation was found to be

TABLE II. Comparison of displacements (in Å), normal to the surface, of atoms in the uppermost trilayer of the clean, partially hydrogenated and fully hydrogenated low index surfaces of anatase, along with the Ti-H and O-H bond lengths.

Surface	Label	Clean	Partial	Full
(001)	$O_{(1)}$	0.20	0.47	0.23
	$Ti_{(2)}$	0.04	0.02	0.12
	$O_{(3)}$	0.05	0.25	0.08
	Ti-H			1.79
	O-H		0.99	1.00
(100)	$O_{(1)}$	0.18	0.36	0.13
	$O_{(2)}$	0.04	0.17	0.00
	$Ti_{(3)}$	−0.16	−0.10	0.07
	Ti-H			1.72
	O-H		0.99	0.99
(101)	$O_{(1)}$	0.06	0.09	0.02
	$O_{(2)}$	0.28	0.43	0.24
	$Ti_{(3)}$	−0.12	−0.06	0.16
	Ti-H			1.74
	O-H		0.98–0.99	0.99

TABLE III. Displacements (in Å), normal to the surface, of atoms in the uppermost trilayer of the low index surface of rutile. Comparisons have been drawn with the DFT LDA results of Ramamoorthy *et al.* (Ref. 48).

Surface	Label	Coordination	This Study	Ref. 48
(001)	$O_{(1)}$	2	0.16	0.06
	$Ti_{(2)}$	4	−0.31	−0.60
	$O_{(3)}$	3	−0.03	−0.08
(100)	$O_{(1)}$	2	0.16	0.01
	$Ti_{(2)}$	5	0.06	−0.14
	$O_{(3)}$	3	0.15	0.03
(110)	$O_{(1)}$	2	−0.19	−0.12
	$Ti_{(2a)}$	6	0.40	0.25
	$Ti_{(2b)}$	5	−0.14	−0.32
	$O_{(3)}$	3	0.24	0.24
(011)	$O_{(1)}$	2	0.09	−0.14
	$Ti_{(2)}$	5	0.05	−0.17
	$O_{(3)}$	3	0.14	0.05

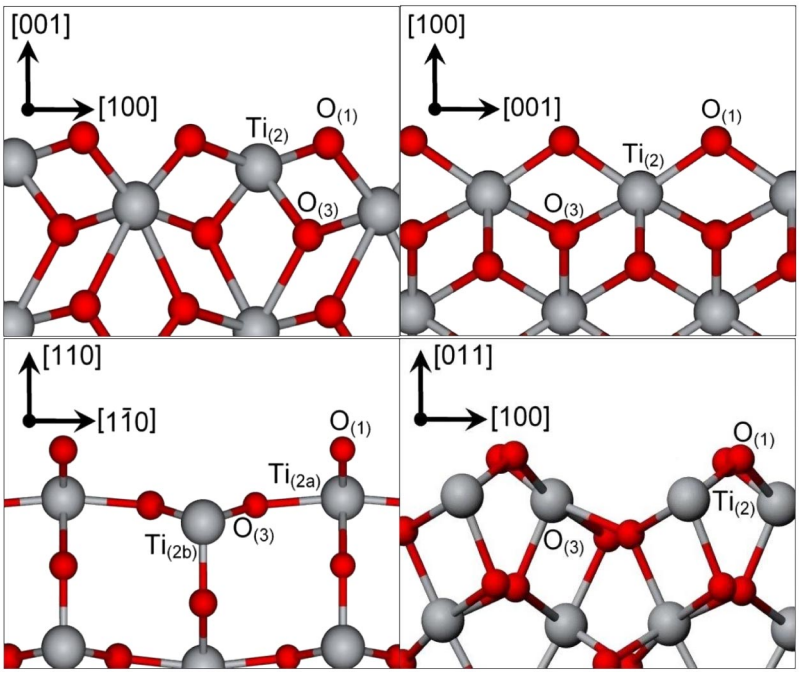

FIG. 5. (Color online) The relaxed rutile (001) surface (top left), (100) surface (top right), (110) surface (lower left), and (011) surface (lower right), with the atoms occupying the atomic layers (denoted by the subscript) of the uppermost trilayer labelled according to Table III.

dominated by an outward relaxation of all atoms, as indicated in Table III in contrast to the results of Ramamoorthy *et al.*[48]

D. H-terminated rutile surfaces

Although a small outward relaxation for the $Ti_{(2)}$ (perpendicular to the surface) is observed in the case of the clean rutile (100) surface, these atoms were found to contract inward in both the partially and fully hydrogenated surfaces (as shown in Fig. 6). This contraction is most significant in the case of the fully hydrogenated surface (see Table IV). The fully hydrogenated rutile (100) surface represents an interesting case. Upon relaxation the hydrogen atoms terminating the $O_{(1)}$ bridging oxygens were found to reorient so that the O-H bonds were directed inward. The resulting $Ti_{(2)}$-$O_{(1)}$-H bond angles were approximately 100.2°. This was combined with the threefold coordinated $O_{(3)}$ atoms relaxing outwards and forming hydrogen bonds with the H atoms, as indicated by the dashed lines in the right image of Fig. 6. This hydrogen bond length was found to be 1.49 Å. In general, this structure reduces the corrugations (or nanofaceting) of the surface.

The (110) surface (see Fig. 7) contains inequivalent (normal to the surface) Ti atoms lying in a centered rectangular arrangement. The atoms denoted as $Ti_{(2a)}$ are sixfold coordinated, while the atoms denoted as $Ti_{(2b)}$ are fivefold coordinated in the clean surface. Around the $Ti_{(2a)}$ atoms chains of twofold coordinated bridging $O_{(1)}$ atoms are aligned along the [001] direction, while rows of threefold coordinated $O_{(3)}$ atoms connect the $Ti_{(2a)}$ and $Ti_{(2b)}$ atoms. The dominant relaxations in this case are those perpendicular to the surface, although the displacement varies with the degree of surface hydrogenation. The bridging $O_{(1)}$ atoms relax outward when H-terminated, but this effect is reduced when the undercoordinated $Ti_{(2b)}$ atoms are also H-terminated. In general, the relaxation of the titanium atoms is most effected by the surface passivation. The difference between the displacements of the $Ti_{(2a)}$ and $Ti_{(2b)}$ atoms is greatest for the clean surface (being 0.40 Å and −0.14 Å, respectively), but this difference diminishes significantly as the hydrogen surface coverage is increased (see Table IV).

The partially hydrogenated rutile (110) surface presented here corresponds to the R model surface reported by Leconte *et al.*,[50] using DFT GGA and Vanderbilt-type pseudopotentials. Although these authors did not report the magnitude of

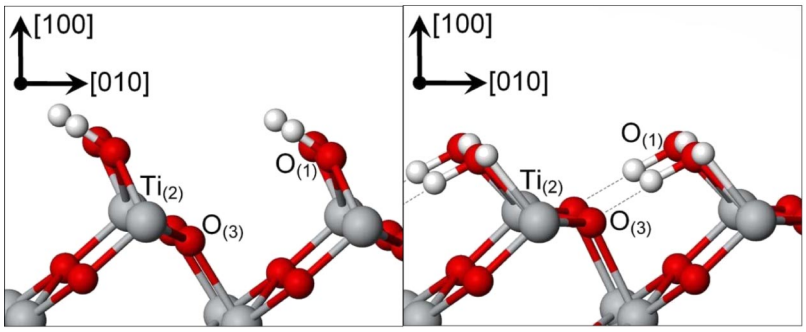

FIG. 6. (Color online) The relaxed, partially hydrogenated rutile (100) surface (left) and fully hydrogenated (100) surface (right). The atoms of the uppermost trilayer labelled according to Table IV (atomic layers are denoted by the subscript).

TABLE IV. Comparison of displacements (in Å), normal to the surface, of atoms in the uppermost trilayer of the clean, partially hydrogenated and fully hydrogenated low index surfaces of rutile, along with the Ti-H and O-H bond lengths.

Surface	Label	Clean	Partial	Full
(100)	$O_{(1)}$	0.16	0.39	0.18
	$Ti_{(2)}$	0.06	−0.04	−0.15
	$O_{(3)}$	0.15	0.36	0.62
	Ti-H			1.80
	O-H		0.99	1.07
(110)	$O_{(1)}$	−0.19	0.27	0.11
	$Ti_{(2a)}$	0.40	0.17	0.02
	$Ti_{(2b)}$	−0.14	−0.15	0.02
	$O_{(3)}$	0.24	0.25	0.15
	Ti-H			1.73
	O-H		0.99	0.99
(011)	$O_{(1)}$	0.09	0.36	0.33
	$Ti_{(2)}$	0.05	−0.04	0.20
	$O_{(3)}$	0.14	0.36	0.07
	Ti-H			1.80
	O-H		1.00	1.02

the relaxation of the surface trilayer with respect the bulk, they did list the O-H bond length as a function of slab thickness. For a slab of nine atomic layers, their O-H bond length of 0.968 Å is slightly smaller than the 0.99 Å listed in Table IV.

Finally, the H-terminated (011) surface was examined, as shown in Fig. 8. Surface hydrogenation was found to affect the magnitude of the surface relaxation, and in the case of the titanium atoms, the direction. The under-coordinated titanium atoms of the partially hydrogenated surface relax inward, but relax outward when H-terminated. In the case of the oxygen atoms, H-termination appears not only to influence the relaxation of the atoms that are capped, but also has a significant effect on the fully coordinated oxygen atoms of the third atomic layer, where the outward relaxation in the partially hydrogenated case is more than double that of the clean surface, but reduced in the fully hydrogenated case (see Table IV).

Like the anatase (110) surface, the rutile (001) surface was found to be unstable to surface hydrogenation, exhibiting bond breaking and symmetry breaking upon relaxation. This instability [like the anatase (110) surface], has been attributed to the fourfold coordinated Ti atoms on the surface.

IV. SURFACE ENERGY AND SURFACE STRESS

The main purpose of the surface component of this study, however, was to obtain a consistent set of surface energy (γ) and surface tension (σ) results. The value of γ was calculated from the energy per TiO_2 unit for the bulk (E^{bulk}) and total energy for the surface (E_N^{surface}) slabs using the expressions

$$\gamma = \frac{G}{A}, \tag{1}$$

$$G = \tfrac{1}{2}(E_N^{\text{surface}} - N\,E^{\text{bulk}} - N_H\,E^H), \tag{2}$$

where G is the free energy of the slab surface, A is the area of the surface, and N is the number of TiO_2 units in the (stoichiometric) cell. The energy of the surface was obtained using the structures described above, and E^{bulk} was obtained from periodic supercell calculations of larger sizes but the same computational conditions. This method has been used successfully before. To account for the surface hydrogenation, N_{H} is the number of terminating hydrogen atoms present on the slab, and their chemical potential $E^H = 1/2E(H_2)$ is half the energy of a free H_2 molecule. Although one value of the hydrogen chemical potential has been used here, in principle, the variation of properties with chemical potential can be easily introduced in this expression.[52]

The value of σ was obtained using the expression

$$\sigma = \frac{\partial G}{\partial A} \approx \frac{\Delta G}{\Delta A}. \tag{3}$$

Therefore, by applying a two-dimensional dilation to the slab in the plane of the surface and calculating the free energy G as indicated in Eq. (1), at each dilation the change in free energy (ΔG) was calculated for a set of area dilations (ΔA). By plotting these results an estimate of the surface tension was obtained from the slope. In this case the intercept should pass through zero (as the change in free energy is zero for an unstressed area), so that any deviation from this condition offered an effective uncertainty.

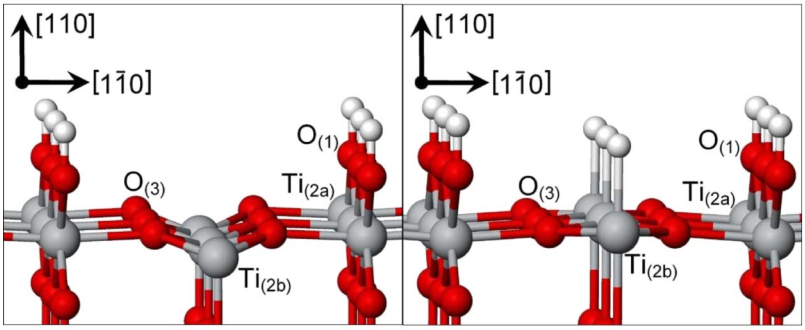

FIG. 7. (Color online) The relaxed, partially hydrogenated rutile (110) surface (left) and fully hydrogenated (110) surface (right). The atoms of the uppermost trilayer labelled according to Table IV (atomic layers are denoted by the subscript).

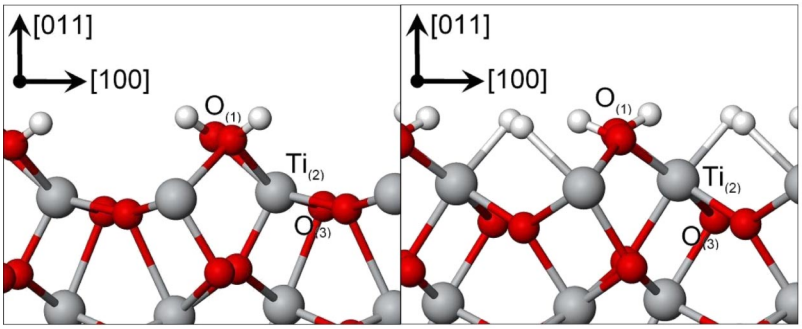

FIG. 8. (Color online) The relaxed, partially hydrogenated rutile (011) surface (left) and fully hydrogenated (011) surface (right). The atoms of the uppermost trilayer labelled according to Table IV (atomic layers are denoted by the subscript).

Three different techniques were undertaken in the calculation of σ for clean surfaces. The first (Method A) involved a uniform dilation (the ratio of the in-plane lattice parameters $x:y$ remained constant), without optimization of the internal parameters. The second approach (Method B) involved a full geometric optimization at each value of ΔA, including the internal parameter, and the in-plane lattice constants. In this approach the $x:y$ ratio changed (although the product $xy = A$ remained constant), resulting in breaking of the symmetry of the slab lattice for each dilation. It is important to note that this procedure also alters the value of γ, as Eq. (1) was applied to the surfaces after the full optimization of the bulk and slab structures. The third method (Method C) involved uniform dilation, *with* optimization of internal parameters but without optimization of the in-plane cell parameters. The results of these calculations, are contained within Tables V and VI for anatase and rutile, respectively.

While values of γ for the low index anatase surface (listed in Table V) are lower than those of Lazerri *et al.*,[46] the order $(101) < (100) < (001) < (110)$ (using each method) is the same. We attribute the lower surface energies in this study in part to the significantly smaller convergence tolerance used for the structural relaxations in our study [10^{-4} eV as opposed to 10^{-2} eV (Ref. 46)], and the use of different GGA methods and the PAW potentials.

Once again, the values of γ (listed in Table VI) for rutile are lower than the values obtained by Ramamoorthy *et al.*[48] (due to the smaller 10^{-4} eV convergence tolerance used for the structural relaxations in our study, as opposed to 10^{-2} eV,[48] and the use of the GGA method with the PAW potentials), however in this case the order is also different. We have obtained the order of $(110) < (100) < (001) < (011)$ (using Methods A and C), as opposed to $(110) < (100) < (011) < (001)$ by Ramamoorthy and colleagues. Note that the order of $(110) < (100) < (011) < (001)$ is different in the case of Method B, due to symmetry breaking during the surface slab optimization.

In general, although the calculation method had little effect on the values of γ, it did have a significant effect upon the surface tension σ for both the anatase and rutile surfaces. This is a result of the stress anisotropy, because the σ_{xy} components are averaged in a different way. For these reasons, we therefore place more confidence in the results obtained using Method C.

The surface energies and surface tensions were however, found to be dependant upon the degree of surface passivation. The results of the hydrogenated surface calculations are contained within Tables VII and VIII for anatase and rutile, respectively. The relative stability of the low index anatase surfaces may be discerned by comparing the values of γ (Table VII). The thermodynamic sequence was found to be the same for the partially hydrogenated and fully hydrogenated anatase surfaces, as for the clean surfaces. Recall that the anatase (110) surface is omitted as it was found to be unstable upon hydrogenation.

The effects of hydrogenation on the surface tension σ of the anatase surface were found to vary considerably. On the (001) surface σ is reduced (with respect to the clean surface) when the surface is partially hydrogenated, but increases again when the titanium atoms are also H-terminated. However, the surface tension of both the (100) and (101) surfaces is lowest when the titanium atoms are terminated. The surface tension of the fully hydrogenated (100) surface was even found to be negative, indicating tendency for this surface to expand (rather than contract) and, if present on the

TABLE V. Comparison of surface free energy γ and surface tension σ (in J/m^2), for the low index surfaces of anatase for the three calculation methods. For comparison the DFT PBE results of Lazerri *et al.* (Ref. 46) are also provided.

	Method A		Method B		Method C		Ref. 46
Surface	γ	σ	γ	σ	γ	σ	γ
(001)	0.51	1.91	0.53	3.79	0.51	2.07	0.90
(100)	0.39	0.58	0.41	0.39	0.39	0.60	0.53
(110)	0.81	0.78	0.82	0.56	0.81	0.73	1.09
(101)	0.35	0.46	0.38	0.38	0.35	0.51	0.44

TABLE VI. Comparison of surface free energy γ and surface tension σ (in J/m^2), for the low index surfaces of rutile for the three calculation methods. For comparison the DFT LDA results of Ramamoorthy *et al.* (Ref. 48) are also provided.

	Method A		Method B		Method C		Ref. 48
Surface	γ	σ	γ	σ	γ	σ	γ
(001)	0.64	0.83	0.44	0.70	0.64	1.02	1.65
(100)	0.60	0.74	0.28	0.76	0.60	0.95	1.12
(110)	0.47	1.17	0.17	1.40	0.47	1.25	0.89, 0.31[a]
(011)	0.95	1.49	0.43	0.92	0.95	1.50	1.40

[a]DFT PBE result of Lazerri *et al.* (Ref. 46).

TABLE VII. Surface free energies γ and surface tensions σ (in J/m^2), for the clean (Method C), partially hydrogenated and fully hydrogenated low index surfaces of anatase.

	Clean		Partial		Full	
Surface	γ	σ	γ	σ	γ	σ
(001)	0.51	2.07	0.86	0.50	0.84	0.91
(100)	0.39	0.60	0.55	0.23	0.65	−0.19
(101)	0.35	0.51	0.51	0.71	0.63	0.09

surface of a nanocrystal, produce a tensile dilation in the direction of the surface normal.

In general the surface energies γ for the rutile surfaces (see Table VIII) are increased by surface hydrogenation. We obtained the order of $(110)<(100)<(011)$ for the partially hydrogenated surfaces and $(110)<(011)<(100)$ for the fully hydrogenated surfaces. Once again, the rutile (001) surface has been omitted as it was found to be unstable to hydrogenation.

The σ of the rutile surfaces (like anatase) is effected by the degree of hydrogenation. In each case the surface tensions of the clean and fully hydrogenated surfaces are closer in magnitude than those of the partially hydrogenated surface. The σ of the partially hydrogenated surfaces are not consistently higher or lower than the corresponding clean and fully hydrogenated surfaces, again indicating that the surface tension of each crystallographic surface of rutile must be calculated explicitly.

Since the compressibility $\beta=1/B_0$ is ultimately required in the phase stability model,[31] the bulk modulus B_0 (and the first derivative of the bulk modulus B_0') were also obtained by fitting calculated energy versus volume curves to the Vinet equation of state.[53] A uniform volume dilation, without optimization of internal parameters (akin to Method A), gave B_0 values of 205 and 233 GPa, and B_0' values of 4.4 and 3.9 for anatase and rutile, respectively. When optimization of internal parameters was included (akin to Method C), superior B_0 values of 190 and 218 GPa, and B_0' values of 4.7 and 4.6 for anatase and rutile were obtained. The latter results are in reasonable agreement with the experimental values of 179 GPa and 4.5 GPa for anatase measured by Arlt *et al.*[54] and of 211 GPa and 6.5 GPa for rutile measured by Gerward and Olsen.[55]

TABLE VIII. Surface free energies γ and surface tensions σ (in J/m^2), for the clean (Method C), partially hydrogenated and fully hydrogenated low index surfaces of rutile.

	Clean		Partial		Full	
Surface	γ	σ	γ	σ	γ	σ
(100)	0.60	0.95	0.71	0.66	1.82	0.80
(110)	0.47	1.25	0.56	1.96	0.84	1.27
(011)	0.95	1.50	1.02	0.39	1.19	1.38

V. PHASE STABILITY

Recently we have proposed a model capable of predicting the free energy of formation of nanocrystals as a function of size, and of nanocrystal shape.[31] The energetically preferred shapes predicted by this model have been found to be in good agreement with experiment in the cases of diamond, silicon, and germanium nanoparticles,[31] and excellent agreement for titanium nitride nanoparticles.[56]

For a given nanoparticle of material x, the free energy may be expressed as a sum of contributions from the particle bulk and surfaces, such that,

$$G_x^o = G_x^{\text{bulk}} + G_x^{\text{surface}}. \tag{4}$$

The free energy of formation of a nanocrystal G_x^o is defined in terms of the surface energy γ_{xi} for each surface i, weighted by the factors f_i, such that $\Sigma_i f_i = 1$. Hence,

$$G_x^o = \Delta_f G_x^o + \frac{M}{\rho_x}(1-e)\left[q\sum_i f_i \gamma_{xi}\right], \tag{5}$$

where $\Delta_f G_x^o$ is the standard free energy of formation of the bulk (macroscopic) material, M is the molar mass, ρ_x is the density and e is the volume dilation induced by the surface tension (which cannot be ignored at the nanoscale). In general, the surface to volume ratio q and the weighting factors f_i must be calculated explicitly for each shape and the facet therein. The effects of edges and corners are omitted here, as they are typically small for nanocrystals larger than ~2 nm, and insignificant for nanocrystals larger than ~5.6 nm.[31] In this size regime it is also possible to make a distinction between the bulk and the surface of the nanoparticle, a division that cannot really be drawn for particles smaller than ~2 nm. It is also important to note that at such small sizes, other types of lattice distortions, such as edge and corner tensions, lattice expansions and contractions and changes in the elastic properties may dominate, and isolated nanocrystals should be treated in their entirety using the appropriate computational technique.[31]

In general, for nanocrystals over ~2 nm we have shown that the volume dilation e due to the surface tension σ may be approximated using the Laplace-Young equation[31] for the effective pressure,

$$P_{\text{eff}} = \frac{2\sigma_x}{R}, \tag{6}$$

where R is the radius of the particle; so that in general (with the compressibility $\beta=1/B_0$),

$$e = \frac{2\beta\sigma_x}{R}. \tag{7}$$

The surface tension is approximated by summing over the (weighted) surface tensions of the crystallographic surfaces present on the nanocrystal,

$$\sigma_x = \sum_i f_i \sigma_{xi}, \tag{8}$$

where σ_{xi} is defined in Eq. (2) and listed in Tables V and VI for $x=$anatase $(\mathcal{A})$ and rutile $(\mathcal{R})$, respectively.

In this model the size dependence is introduced not only by the reduction of e as the crystal grows larger, but also by the surface to volume ratio q. The shape dependence is also

introduced by q, as well as the weighted sums of the surface energies and the surface stresses, corresponding to the surfaces present in the particular morphology of interest.

Previously it has been determined that the Laplace-Young description of the pressure is suitable in the case of faceted nanocrystals.[31] This approach has been rigorously compared to the more general Stoneham model,[57] and found to give a good description of the volume dilation in facetted nanocrystals over ~2 nm. Therefore, the surface energies and surface tensions for each surface facet i, along with the molar mass of TiO_2, the density of anatase and rutile ($\rho_{\mathcal{A}}=3.893$ g/cm^3 and $\rho_{\mathcal{R}}=4.249$ g/cm^3) and the standard free energies of formation[58] ($\Delta_f G^o_{\mathcal{A}}$ and $\Delta_f G^o_{\mathcal{R}}$) are all that is required to compare the phase stability of faceted TiO_2 nanocrystals over ~2 nm.

All of the calculations in the present study have been performed at $T=0$, so that G^o_x is equivalent to the enthalpy of formation. It has been shown by Zhang and Banfield[11] that the change in the surface energies with temperature is of the order of 10^{-4} J/m^2, so it has been assumed here that variations in the equilibrium morphology of anatase and rutile nanocrystals due to temperature effects will be negligible.

A. Phase stability of faceted TiO_2 nanocrystals

The shapes of the clean anatase and rutile nanocrystals compared in this study were identified by generating the Wulff construction[59] for each material, using the surface energies contained within Tables V and VI, respectively. The values of γ calculated using each Method (A, B, and C) varied so little as to make variations in the corresponding Wulff construction undiscernible. Therefore, the Wulff crystal shapes shown in at the top of Fig. 9 correspond to the minimum energy morphology calculated in this study, irrespective of method.

For each of the methods described above, the value of G^o_x (where $x=\mathcal{A},\mathcal{R}$) was calculated and plotted as a function of the number of TiO_2 units, and the points of intersection determined. An example of this plot is shown in Fig. 10 for Method C. For each Method A, B, and C the intersection points were found to occur at ~12 600, ~12 400, and ~12 300 TiO_2 units, respectively. This corresponds to anatase nanocrystals with average diameters of ~9.4, ~9.3, and ~9.3 nm, or apex-to-apex lengths of ~20.1, ~20.0, and ~19.9 nm; and rutile nanocrystals with average diameters of ~9.1, ~9.0, and ~9.0 nm, or apex-to-apex lengths of ~13.3, ~13.2, and ~13.2 nm, respectively.

Therefore, the intersection point (at which the phase transition is identified) was found to vary little with the method used to calculate the surface stress, even though the values of σ were (in general) found to be reasonably sensitive to the method of approximation. The phase transition point of 9.3–9.4 nm in (average) diameter is also in excellent agreement with the average diameter of 9.3 nm predicted by Zhang and Banfield[11] model at 0 K. This may however be fortuitous, since the Zhang and Banfield model assumed that both the anatase and rutile nanocrystals are spherical; and as mentioned above, the model does not account for the differing number of atoms in anatase and rutile crystals of the same diameter. Their findings are also based on surface energies obtained using empirical[47] rather than *ab initio* methods, as we have done here.

In order to investigate the issue for spherical nanoparticles, the model presented herein was also applied to spheres of TiO_2. This was achieved by inputting a sphere as the shape of interest into Eq. (4), and using averages of the surface energy and surface stress, averaging over all the low index surfaces of anatase or rutile. The results are shown in Fig. 11. It is clear from these results that not only is it important to explicitly consider the number of TiO_2 units, but the description of facetted nanocrystals is crucial to obtain a value of size at the phase transition that correlates well with experiment. The free energy of the spherical nanoparticles is considerably higher than that of the facetted nanocrystal, in both cases of anatase and rutile, and the phase transition of spherical nanoparticles is predicted to occur at just 270 TiO_2 units. This point corresponds to an anatase nanoparticle of only ~2.6 nm in diameter.

Experimentally, the transition point at ~650–800 K for hydrothermally prepared samples has been predicted to be at approximately 11.4–17.6 nm, but has been found to decrease with temperature.[10] The discrepancy between the calculated transition size and the experimental size may be attributed to a number of factors. First, the experimental samples were analyzed in solution whereas the present study

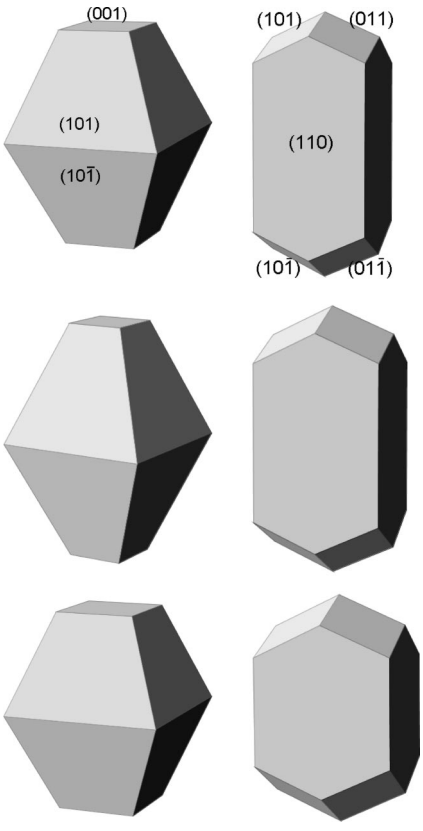

FIG. 9. Wulff constructions for clean (top), partially hydrogenated (center), and fully hydrogenated (bottom) anatase (left) and rutile (right) calculated using the surface free energies listed in Tables VII and VIII.

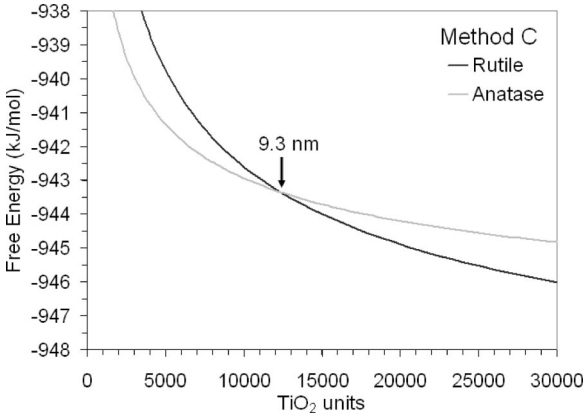

FIG. 10. Free energy as a function of number of TiO_2 units for anatase and rutile, calculated using the shapes given at the top of Fig. 9 and the values of γ and σ obtained using Method C. The intersection points indicate the phase transition.

considers nanoparticles under vacuum conditions. Second, the experimental measurements were undertaken at finite temperature, whereas the calculations of the surface energies and tensions here were performed at $T=0$, and as mentioned above the transition size (experimentally) was found to decrease with temperature.[10] Finally, the experimental conditions may not have been at thermodynamic equilibrium, implying that nonequilibrium shapes may have been involved. The importance of the latter should not be underestimated. As the present study clearly shows, the shape of the nanocrystals may alter the phase stability significantly.

B. Effects of surface hydrogenation

The remaining Wulff crystal shapes shown in Fig. 9 correspond to the minimum energy morphology obtained from the surface energies calculated in this study for partially hydrogenated (top) and fully hydrogenated (bottom) surfaces. Although the degree of hydrogenation has almost no effect on the minimum energy shape of the anatase nanocrystal, the

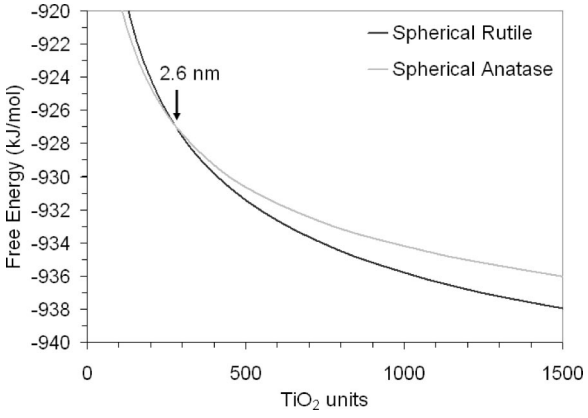

FIG. 11. Free energy as a function of number of TiO_2 units for spherical anatase and rutile nanoparticles, calculated using the values of γ and σ averaged over surface orientations. The intersection point indicates the phase transition (all results obtained using Method C).

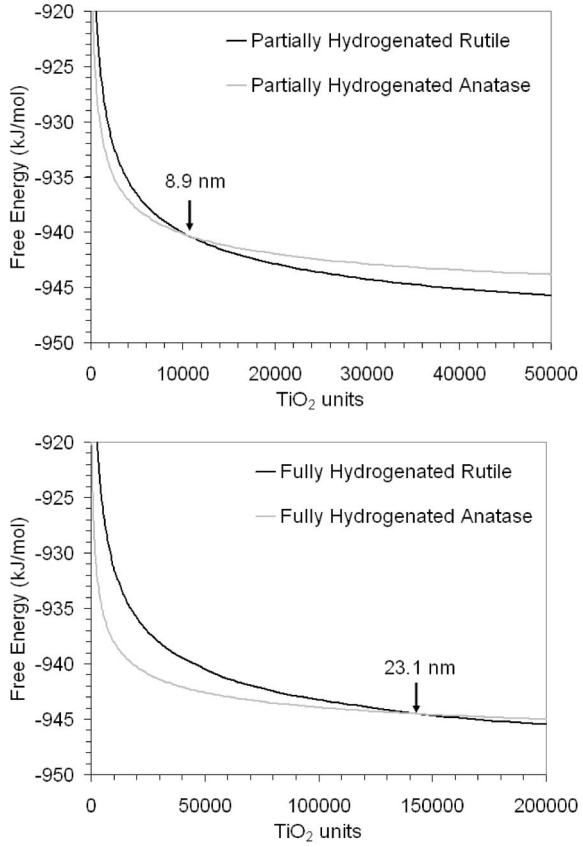

FIG. 12. Free energy as a function of number of TiO_2 units for anatase and rutile, calculated using the shapes given in Fig. 9 and the values of γ and σ from Table VII and VIII for partially hydrogenated surfaces (top) and fully hydrogenated surfaces (bottom). The intersection points indicate the phase transition. The sizes indicated by the arrows refer to the average diameters of anatase nanocrystals.

effect of surface hydrogenation on the shape of rutile at the nanoscale is clearly evident. Clean rutile surfaces produce longer prismatic crystals, whereas the crystals become more stunted as the amount of surface hydrogen is increased; finally resulting in a squat crystal that is almost as wide as it is tall (along the a and b axes) when all under-coordinated atoms are terminated.

For each of the nanocrystals above, the value of $G^o_{\mathcal{A}}$ and $G^o_{\mathcal{R}}$ were calculated and plotted as a function of the number of TiO_2 units, by using the appropriate surface energies from Tables VII and VIII. By determining each point of intersection, the phase stability of the faceted nanocrystals was investigated as a function of surface hydrogenation. These plots are shown in Fig. 12 for the partially hydrogenated (top) and fully hydrogenated (bottom) surfaces. The intersection points were found to occur at ~10 800 and ~196 900 TiO_2 units, respectively. This corresponds to nanoanatase crystals with average diameters of ~8.9 nm and ~23.1 nm, or apex-to-apex lengths of ~19.1 nm and ~49.8 nm; and nanorutile crystals with average diameters of ~8.6 nm and ~22.2 nm, or apex-to-apex lengths of ~10.4 nm and ~41.2 nm, respectively. Note that the apex-to-apex distance

varies as a function of the phase transition point and the shape of the nanocrystal in the case of rutile.

This dramatic change indicates that the termination of under-coordinated surface sites plays a major role in determining the stability of nanoscale TiO_2, as we have shown for the case of H-termination. Full hydrogenation of the nanocrystal surfaces is predicted to promote stability of the anatase phase, whereas hydrogenation of only the bridging oxygens (partial hydrogenation) promotes stability of the rutile phase.

VI. CONCLUSIONS

Using a complete set of values for the surface energy and surface tension of low index anatase and rutile surfaces, calculated using DFT GGA with the PAW potential method, and a model to describe the free energy of nanocrystals as a function of size and shape, the relative phase stability of faceted TiO_2 nanocrystals has been investigated. The results predict, at low temperatures, a phase transition point at an average diameter of approximately 9.3–9.4 nm (9.0–9.1 nm) for anatase (rutile) nanocrystals. It has also been shown that the arbitrary description of TiO_2 nanoparticles as spheres is not valid, as it does not represent the minimum energy morphology, nor does it reproduce the correct size regime of the phase transition.

This study also predicts that the shape of anatase is independent of the degree of surface hydrogenation (as shown by the corresponding Wulff construction for various degrees of surface coverage), but that rutile crystals become more squat as the coverage by hydrogen is increased. This is an example of the shape (as distinct from phase) of the nanocrystals being effected by the chemical environment (in this case, hydrogen), but implications of a medium such as a matrix or surrounding nanoparticles still need to be addressed.

Further, the results show that (at low temperatures) the anatase-to-rutile phase transition size also depends on the surface passivation. Compared with the results for clean surfaces, the transition size decreases slightly to 8.9 nm when the surface bridging oxygens are H-terminated, but increases significantly to 23.1 nm when both the bridging oxygens and under-coordinated titanium atoms of the surface trilayer are H-terminated. This is consistent with experimental findings that indicate that the transition energy and size vary depending upon factors such as reaction atmosphere and synthesis conditions.[17,60–63]

Further work is currently underway to examine the effects of pH on the anatase and rutile size and shape, and on the phase transition point.

ACKNOWLEDGMENTS

This work has been supported by the U.S. Department of Energy, BES-Chemical Sciences, under Contract No. W-31-109-ENG-38. Computational resources for this project have been supplied by Argonne National Laboratory–Laboratory Computing Resource Center, Pacific Northwest National Laboratory Molecular Science Computing Facility and the U.S. Department of Energy National Energy Research Scientific Computing Center. The authors would also like to acknowledge Larry A. Curtiss for useful discussions.

*Electronic address: amanda.barnard@anl.gov
†Electronic address: zapol@anl.gov

[1] W. F. Zhang, M. S. Zhang, Z. Yin, and Q. Chen, Appl. Phys. B: Lasers Opt. **B70**, 261 (2000).
[2] T. Rajh, L. X. Chen, L. Lucas, T. Liu, M. C. Thurnauer, and D. M. Tiede, J. Phys. Chem. B **106**, 10543 (2002).
[3] T. Paunesku, T. Rajh, G. Wiederrecht, J. Maser, S. Vogt, N. Stojićević, M. Protić, B. Lai, J. Oryhon, M. Thurnauer, and G. Woloschak, Nat. Mater. **2**, 343 (2003).
[4] L. C. Chen, T. Rajh, W. Jäger, J. M. Nedeljkovic, and M. C. Thurnauer, J. Synchrotron Radiat. **6**, 455 (1999).
[5] T. Rajh, J. M. Nedeljkovic, L. C. Chen, O. Poluektov, and M. C. Thurnauer, J. Phys. Chem. B **103**, 3515 (1999).
[6] K. D. Jang, S.-K. Kim, and S.-J. Kim, J. Nanopart. Res. **3**, 141 (2001).
[7] H. Bullen and S. Garrett, Nano Lett. **2**, 739 (2002).
[8] H. Zhang, R. L. Penn, R. J. Hamers, and J. F. Banfield, J. Phys. Chem. B **103**, 4656 (1999).
[9] J. Muscat, V. Swamy, and N. M. Harrison, Phys. Rev. B **65**, 224112 (2002).
[10] A. A. Gribb and J. F. Banfield, Am. Mineral. **82**, 717 (1997).
[11] H. Zhang and J. F. Banfield, J. Mater. Chem. **8**, 2073 (1998).
[12] M. R. Rande, A. Navrotsky, H. Z. Zhang, J. F. Banfield, S. H. Elder, A. Zaban, P. H. Borse, S. K. Kulkarni, G. S. Doran, and H. J. Whitfield, Proc. Natl. Acad. Sci. U.S.A. **99**, 6481 (2002).
[13] H. Zhang and J. F. Banfield, J. Phys. Chem. B **104**, 3491 (2000).
[14] H. Zhang and J. F. Banfield, Am. Mineral. **84**, 528 (1999).
[15] H. Zhang and J. F. Banfield, J. Mater. Res. **15**, 437 (2000).
[16] T. B. Ghosh, S. Dhabal, and A. K. Datta, J. Appl. Phys. **94**, 4577 (2003).
[17] S. Kittaka, K. Matsuno, and S. Takahara, J. Solid State Chem. **132**, 447 (1997).
[18] H. Zhang, M. Finnegan, and J. F. Banfield, Nano Lett. **1**, 81 (2001).
[19] M. Sugiyama, H. Okazaki, and S. Koda, Jpn. J. Appl. Phys., Part 1 **41**, 4666 (2002).
[20] T. Sugimoto, X. Zhou, and A. Muramatsu, J. Colloid Interface Sci. **259**, 43 (2003).
[21] P. I. Gourma and M. J. Mills, J. Am. Ceram. Soc. **84**, 619 (2001).
[22] Y. Li, T. White and S. H. LimRev. Adv. Mater. Sci. **5**, 211 (2003).
[23] R. Arroyo, G. Córdoba, J. Padilla, and V. H. Lara, Mater. Lett. **54**, 397 (2002).
[24] J. Arbiol, J. Cerdà, G. Dezanneau, A. Cirera, F. Peiró, A. Cornet, and J. R. Morante, J. Appl. Phys. **92**, 853 (2002).
[25] M. S. P. Francisco and V. R. Mastelaro, Chem. Mater. **14**, 2514 (2002).
[26] T. Sugimoto, K. Okada, and H. Itoh, J. Colloid Interface Sci. **193**, 140 (2003).
[27] T. Sugimoto, X. Zhou, and A. Muramatsu, J. Colloid Interface Sci. **259**, 53 (2003).

[28] Y. Gao and S. A. Elder, Mater. Lett. **44**, 228 (2000).
[29] R. L. Penn and J. F. Banfield, Geochim. Cosmochim. Acta **63**, 1549 (1999).
[30] S. T. Aruna, S. Tirosh, and A. Zuban, J. Mater. Chem. **10**, 2388 (2000).
[31] A. S. Barnard and P. Zapol, J. Chem. Phys. **121**, 4276 (2004).
[32] U. Diebold, Surf. Sci. Rep. **48**, 53 (2003).
[33] V. E. Henrich and R. L. Kurtz, Phys. Rev. B **23**, 6280 (1981).
[34] J.-M. Pan, B. L. Maschhoff, U. Diebold, and T. E. Madey, J. Vac. Sci. Technol. A **10**, 2470 (1992).
[35] H. M. Lu, W. X. Zhang, and Q. Jiang, Adv. Eng. Mater. **5**, 787 (2003).
[36] J. P. Perdew and Y. Wang, Phys. Rev. B **45**, 13 244 (1992).
[37] G. Kresse and J. Hafner, Phys. Rev. B **47**, 558 (1993).
[38] G. Kresse and J. Furthmüller, Phys. Rev. B **54**, 11 169 (1996).
[39] G. Kresse and J. Furthmüller, Comput. Mater. Sci. **6**, 15 (1996).
[40] D. M. Wood and A. Zunger, J. Phys. A **18**, 1343 (1985).
[41] D. Vanderbilt, Phys. Rev. B **41**, 7892 (1990).
[42] G. Kresse and J. Hafner, J. Phys.: Condens. Matter **6**, 8245 (1994).
[43] P. E. Blöchl, Phys. Rev. B **50**, 17 953 (1994).
[44] G. Kresse and D. Joubert, Phys. Rev. B **59**, 1758 (1999).
[45] A. Beltrán, J. R. Sambrano, M. Calatayud, F. R. Sensato, and J. Andrés, Surf. Sci. **490**, 116 (2001).
[46] M. Lazzeri, A. Vittadini, and A. Selloni, Phys. Rev. B **63**, 155409 (2001); **65**, 119901 (2002).
[47] P. M. Oliver, G. W. Watson, E. T. Kelsey, and S. C. Parker, J. Mater. Chem. **7**, 563 (1997).
[48] M. Ramamoorthy, D. Vanderbilt, and R. D. King-Smith, Phys. Rev. B **49**, 16 721 (1994).
[49] V. Swamy, J. Muscat, J. D. Gale, and N. M. Harrison, Surf. Sci. **504**, 115 (2002).
[50] J. Leconte, A. Markovits, M. K. Skalli, C. Minot, and A. Belmajdoub, Surf. Sci. **497**, 194 (2002).
[51] G. Charlton, P. B. Howes, C. L. Nicklin, P. Steadman, J. S. G. Taylor, C. A. Muryn, S. P. Harte, J. Mercer, R. McGrath, D. Norman, T. S. Turner, and G. Thornton, Phys. Rev. Lett. **78**, 495 (1997).
[52] K. Reuter and M. Scheffler, Phys. Rev. B **65**, 035406 (2002).
[53] P. Vinet, J. H. Rose, J. Ferrante, and J. R. Smith, J. Phys.: Condens. Matter **1**, 1941 (1989).
[54] T. Arlt, M. Bermejo, M. A. Blanco, L. Gerward, J. Z. Jiang, J. S. Olsen, and J. M. Recio, Phys. Rev. B **61**, 14 414 (2000).
[55] L. Gerward and J. S. Olsen, J. Appl. Crystallogr. **30**, 259 (1997).
[56] A. S. Barnard, J. Comp. Theo. Nanosci. (to be published).
[57] A. M. Stoneham, J. Phys. C **10**, 1175 (1977).
[58] The experimental values of the free energies of formation of anatase and rutile $\Delta_f G^o_{\mathcal{A}}$ and $\Delta_f G^o_{\mathcal{R}}$ taken from the JANAF tables (for the case where $T=0$) have been applied here, such that $\Delta_f G^o_{\mathcal{A}} = -9.491\,471 \times 10^{-2}$ mJ/mol and $\Delta_f G^o_{\mathcal{R}} = -9.539\,962 \times 10^{-2}$ mJ/mol. M. W. Chase, C. A. Davies, J. R. Downey, D. J. Frurip, R. A. McDonald, and A. N. Syverud, J. Phys. Chem. Ref. Data **14** (Suppl. 1), 1680 (1985).
[59] G. Wulff, Z. Kristallogr. Mineral. **34**, 449 (1901).
[60] M. Yoshinaka, K. Hirota, and O. Yamaguchi, J. Am. Ceram. Soc. **80**, 2749 (1997).
[61] K. Okada, N. Yamamoto, Y. Kameshima, and A. Yasumori, J. Am. Ceram. Soc. **84**, 1591 (2001).
[62] J. Yang, S. Mei, and J. M. F. Ferreira, J. Am. Ceram. Soc. **83**, 1361 (2000).
[63] A. Zaban, S. T. Aruna, S. Tirosh, B. A. Gregg, and Y. Mastai, J. Phys. Chem. B **104**, 4130 (2000).